

Cite this: *Nanoscale*, 2016, 8, 15486Received 1st April 2016,
Accepted 2nd August 2016

DOI: 10.1039/c6nr02715f

www.rsc.org/nanoscale

One-step synthesis and luminescence properties of tetragonal double tungstates nanocrystals†

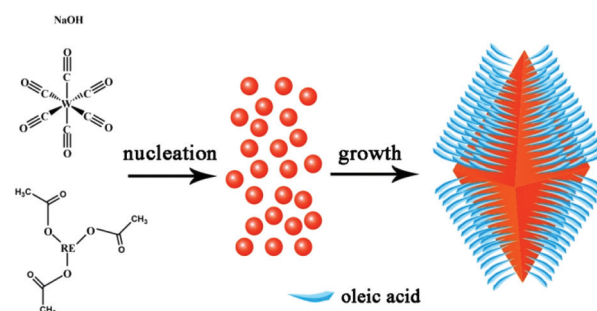
Z. J. Wang,^{a,b} Y. L. Zhang,^a J. P. Zhong,^{*a} H. H. Yao,^a J. Wang,^a M. M. Wu^a and A. Meijerink^b

A versatile one-step thermolysis protocol is demonstrated to produce a uniform dispersion of tetragonal double tungstates NaRE(WO₄)₂ (RE = rare earth) nanocrystals (NCs). Oriented attachment in the [001] direction occurred. Doping with luminescent RE³⁺ ions resulted in highly luminescent NCs showing characteristic line emission of the dopant as well as a blue emission assigned to surface adsorbed organic species.

Nanocrystals (NCs) doped with rare-earth (RE) ions can have high luminescence efficiency, characteristic sharp line emission, low toxicity, high physical and chemical stabilities and have therefore attracted much attention for applications in bio-detection, bio-imaging, drug delivery, tumor diagnosis and therapeutics.^{1–3} In the past few decades, extensive synthetic work concerning RE-doped NCs has been carried out for binary and ternary compounds.^{4,5} However, there are only a few reports on NCs in more complicated quaternary systems. The double tungstates with the formula MRE(WO₄)₂ (M = alkali metals) are excellent hosts for luminescent materials for applications in lighting, displays, lasers and scintillators.⁶ These double salts possess compact packing of the crystal lattice, giving outstanding chemical and physical stabilities, which is an important requirement of functional materials. A variety of synthesis protocols have been reported including solid state reactions,⁷ liquid phase methods,^{8,9} and single crystal growth.¹⁰ Different synthesis methods have resulted in highly luminescent macro- and microcrystalline materials of varying sizes and shapes with luminescent dopant ions as Eu³⁺, Tb³⁺ and Er³⁺. However, monodisperse MRE(WO₄)₂ nanomaterials with crystal sizes below 50 nm have never been reported and especially for applications in bio-imaging these

small sizes are essential. To our knowledge, this study presents the first successful attempt to prepare uniform tetragonal double tungstates NaRE(WO₄)₂ NCs with sizes smaller than 50 nm by a one-step thermolysis method. Oriented attachment was observed to occur for these small diamond-shaped NCs. The photoluminescence properties of the as-synthesized NCs were investigated and compared with those of bulk NaLa(WO₄)₂:Eu³⁺ (microcrystals, MCs).

The NaRE(WO₄)₂ NCs were produced by a one-step thermolysis method with a special precursor of hexacarbonyl tungsten (see the Experimental section in the ESI† for details). The process for NaRE(WO₄)₂ NC growth is displayed in Scheme 1. This synthesis methodology was used to prepare NaLa(WO₄)₂ NCs with different Eu³⁺-doping concentrations. The X-ray diffraction (XRD) patterns shown in Fig. 1 reveal that all the diffraction peaks of samples are characteristic of the tetragonal structure (JCPDS 79-1118: NaLa(WO₄)₂, *a* = *b* = 5.349 Å, *c* = 11.628 Å, space group *I*₄/a). Recent research has shown that the correct space group is *I* $\bar{4}$ with two different crystal sites shared by Na and RE instead of *I*₄/a with only a single shared site for Na and RE.^{10–12} Note that although the space group in the JCPDS file is not correct, the position of the diffraction peaks is not affected. The peak broadening is ascribed to the nano-size of the particles. In addition, a series of NaRE(WO₄)₂ (RE = Y, La–Lu) were produced. The XRD diffractograms in



Scheme 1 Schematic display of the synthesis strategy for NaRE(WO₄)₂ NCs.

^aMOE Laboratory of Bioinorganic and Synthetic Chemistry, KLGEI of Environment and Energy Chemistry, State Key Laboratory of Optoelectronic Materials and Technologies, School of Chemistry and Chemical Engineering, Sun Yat-sen University, Guangzhou 510275, China. E-mail: zhongjp@mail.sysu.edu.cn

^bCondensed Matter and Interfaces, Debye Institute for Nanomaterials Science, Utrecht University, Princetonplein 1, 3584 CC Utrecht, Netherlands

†Electronic supplementary information (ESI) available. See DOI: 10.1039/c6nr02715f

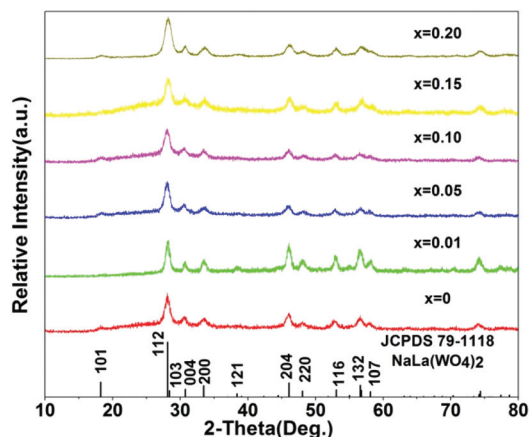


Fig. 1 XRD patterns of $\text{NaLa}_{1-x}\text{Eu}_x(\text{WO}_4)_2$ ($x = 0, 0.01, 0.05, 0.10, 0.15, 0.20$) NCs.

Fig. S1† demonstrate the applicability of this preparation method to all RE elements for the synthesis of nanocrystalline $\text{NaRE}(\text{WO}_4)_2$ compounds. The decrease of unit cell parameters in $\text{NaRE}(\text{WO}_4)_2$ along the RE series induces the shift of diffraction peaks towards higher angles, in agreement with the decreasing ionic radii of the RE ions along the lanthanide series.

The transmission electron microscopy (TEM) images of $\text{NaLa}_{0.9}\text{Eu}_{0.1}(\text{WO}_4)_2$ NCs and other double tungstates are displayed in Fig. 2 and S2,† respectively. Analysis of the TEM images reveals that monodisperse diamond shaped $\text{NaRE}(\text{WO}_4)_2$ NCs of $12 \pm 1 \text{ nm} \times 29 \pm 1 \text{ nm}$ with a small size distribution can be produced through the synthesis method used. Crystals of similar morphology with sizes over 100 nm have been obtained by using a hydrothermal method.^{8,13} The hydrothermal synthesis route allows for size variation but has not been able to produce monodisperse sub-50 nm nanoparticles. The thickness of the NCs was determined to be 2–3 nm *via* atomic force microscopy (AFM) presented in Fig. S3.† The elemental composition of the product was confirmed by energy-dispersive X-ray spectroscopy (EDS, inset of Fig. 2a), where the Cu signal is from the carbon-copper grid. In the high resolution TEM image of a single NC shown in Fig. 2b,

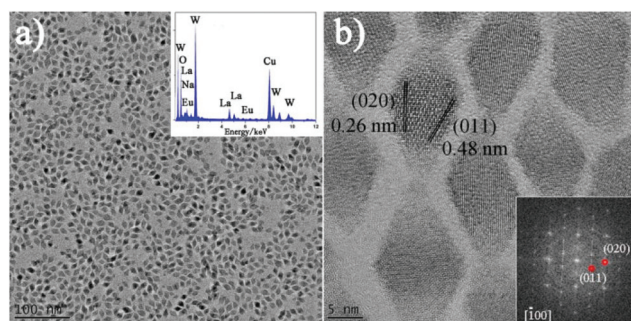


Fig. 2 TEM images of $\text{NaLa}_{0.9}\text{Eu}_{0.1}(\text{WO}_4)_2$ NCs in different magnifications. The insets are: (a) EDS spectrum and (b) FFT analysis.

lattice planes can be observed with lattice spacings of 0.26 and 0.48 nm which can be indexed as (020) and (011) planes. Based on the orientation of these lattice planes it can be derived that the crystal is bound to $\{110\}$ facets with the [001] orientation along two vertices. This orientation is further verified by the fast Fourier transform (FFT) analysis shown in the inset of Fig. 2b, when viewed from the [100] direction. Since the surface energy of the (001) facets is higher than that of the $\{110\}$ ones,¹⁴ the (001) facets are prone to diminish, even vanish, leaving behind the $\{110\}$ facets to define the morphology of the crystals.

The phenomenon of oriented attachment of the NCs was observed for the samples obtained from the concentrated NCs dispersed in toluene. Fig. 3a exhibits a large area with a monolayer of ordered NCs. The magnified image (Fig. 3b) demonstrates a parallel alignment of elongated chains and each chain consists of a number of ultrathin NCs with chain lengths up to hundreds of nanometers. Adjacent NCs align along the [100] direction by means of attachment to each other *via* the (001) facets, driven by the reduction of surface energy and inherently anisotropic growth of the tetragonal phase. In contrast, the NCs synthesized using the RE ion (iii) acetylacetonate precursors also show oriented attachment (Fig. 3c and d), but these aggregates have irregular surfaces as well as shorter alignment lengths. The corresponding NCs form small clusters *via* oriented attachment and are no longer visible as an individual NC. Therefore, we speculate that the (001) facets of a single NC in the case of the RE-acetylacetonate precursor contain a higher proportion of exposed facets in comparison with the situation for the RE-acetate precursor. The difference in the decomposition rate and activity of the two RE^{3+} precursors may account for the different extents of exposed (001) facets as well as nucleation and growth of the NCs. The schematic is illustrated in Fig. 3e for the proposed oriented attachment of $\text{NaLa}(\text{WO}_4)_2$ NCs *via* the (001) facets.

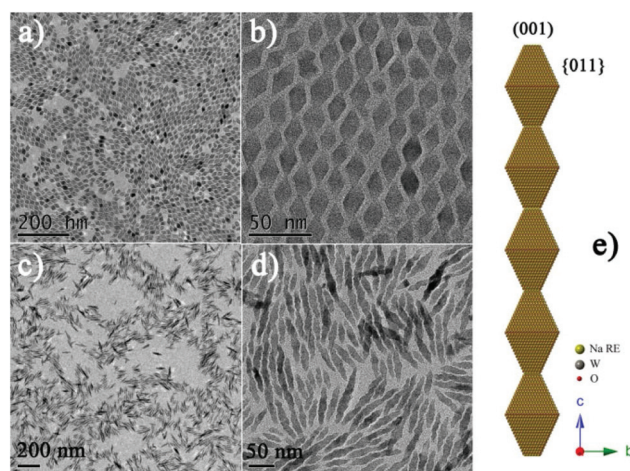


Fig. 3 TEM images of $\text{NaLa}_{0.9}\text{Eu}_{0.1}(\text{WO}_4)_2$ NCs in different resolutions, prepared using RE-acetate (a, b) and RE-acetylacetonate (c, d) precursors, respectively. (e) The atomic reconstruction of five NCs showing oriented attachment.

The as-synthesized NCs were used to investigate their unique luminescence behavior. Fig. S4† depicts the excitation spectra at various temperatures while monitoring the Eu^{3+} f-f emission at 614 nm. The excitation spectrum shows sharp lines between 350 and 550 nm. In addition a strong broad excitation band was observed between 250 and 300 nm as well as a broad shoulder extending from 300 to 400 nm. The narrow peaks are assigned to the f-f transitions of Eu^{3+} and are located at the characteristic wavelength for Eu^{3+} (see the assignment in Fig. S4†). The broad band around 270 nm was also observed in bulk $\text{NaLa}(\text{WO}_4)_2:\text{Eu}^{3+}$ and is assigned to the charge transfer band (CTB) of the host $\text{O}^{2-}-\text{W}^{6+}$, possibly overlapping with an $\text{O}^{2-}-\text{Eu}^{3+}$ CTB, which is also expected in this spectral region. The broad band around 350 nm is not observed in bulk $\text{NaLa}(\text{WO}_4)_2:\text{Eu}^{3+}$. In the past, a near UV absorption band (and blue emission) has been reported for NCs prepared in the presence of organic molecules like oleic acid.¹⁵ The origin of the emitting species is not clear but is well known that during synthesis procedures at elevated temperatures in the presence of organic capping molecules, luminescent molecules can be formed with an extended conjugated π -system giving rise to visible emission upon UV excitation.¹⁶ In our system, the presence of a surface capping oleate ligand is confirmed by the Fourier transform infrared (FT-IR) spectrum in Fig. S5.† The observation of the near UV band in the excitation spectrum of the Eu^{3+} emission suggests that there is an energy transfer from the organic luminescent species to the 4f states of Eu^{3+} providing additional evidence that this species is adsorbed at the NC surface in close proximity to Eu^{3+} ions. The intensities of the two broad bands and excitation peaks continuously decrease as temperature increases, in agreement with the discussion on the thermal quenching of the corresponding emission (*vide infra*). Note that the hot band from the $^7\text{F}_1-^5\text{D}_1$ transition increases its intensity until 280 K as a result of thermal population of the $^7\text{F}_1$ state. The emission spectrum of Eu^{3+} -doped $\text{NaLa}_{0.9}\text{Eu}_{0.1}(\text{WO}_4)_2$ NCs is shown in Fig. 4a together with an emission spectrum for the microcrystalline analogue (Fig. 4b) for comparison. The microcrystalline material was produced by the solid state method described in our previous work.⁷ Both the emission spectra show the characteristic Eu^{3+} emission peaks around 590 nm ($^5\text{D}_0-^7\text{F}_1$), 610 nm ($^5\text{D}_0-^7\text{F}_2$) and 700 nm ($^5\text{D}_0-^7\text{F}_4$). The spectra are very similar, as expected since the local environment determined by the crystal structure is the same for Eu^{3+} in the NCs and MCs, while the spectra for Eu^{3+} in the MCs show slightly sharper emission lines. Analysis of high resolution emission spectra (Fig. S6†) recorded at low temperature (4 K) shows that the full width at half maximum (FWHM) of the two dominant $^5\text{D}_0-^7\text{F}_2$ emission peaks at ~ 610 and 613 nm is 0.6 and 1.0 nm for the MCs and 0.9 and 2.2 nm for the NCs. This is explained by a larger inhomogeneous broadening for the Eu^{3+} emission in the NC sample where variations in the local environment of Eu^{3+} due to (surface) disorder will give rise to more inhomogeneous broadening in the nanocrystalline material. Note that also for the Eu^{3+} in the MCs the linewidth is relatively broad due to the cation disorder in the crystal

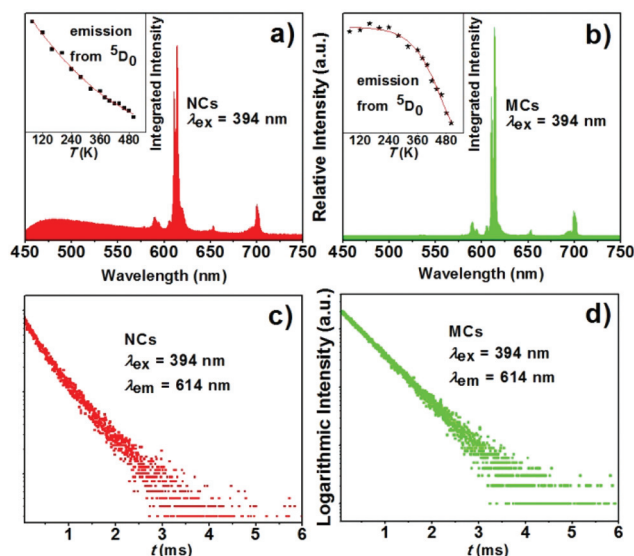


Fig. 4 The emission spectra ($\lambda_{\text{ex}} = 394$ nm) of (a) $\text{NaLa}_{0.9}\text{Eu}_{0.1}(\text{WO}_4)_2$ NC and (b) MC counterparts, and (c, d) corresponding decay curves ($\lambda_{\text{ex}} = 394$ nm and $\lambda_{\text{em}} = 614$ nm) at 300 K. The insets in (a, b) show the integrated emission intensity from the $^5\text{D}_0$ state versus temperature.

structure.¹¹ In the emission spectrum for the nanocrystalline material a broad emission band was also observed in the blue spectral region, which is consistent with the observation of the broad band in the excitation spectrum between 300 and 400 nm. The temperature dependent emission spectra were measured in the range of 77–500 K. When excited at 394 nm ($^7\text{F}_0-^5\text{L}_6$), the emission of Eu^{3+} in both the NC and MC materials shows thermal quenching. The insets in Fig. 4a and b show the temperature dependence of the integrated emission intensity. For Eu^{3+} in the NCs there is a continuous decrease in intensity between 77 and 500 K. For Eu^{3+} in the MCs the onset of the quenching is around 350 K, where the quenching behavior reflects the intrinsic quenching for Eu^{3+} in this host material. For Eu^{3+} in the NCs there is an additional thermally activated non-radiative decay process that may be related to thermally activated energy transfer to (surface) defects or the surface adsorbed organic species.

The luminescence decay curves are shown in Fig. 4c and d, by recording the $^5\text{D}_0-^7\text{F}_2$ emission at room temperature. In the MCs a single exponential decay was observed with a decay time of 0.54 ms, which reflects the radiative decay rate for the $^5\text{D}_0$ state of Eu^{3+} in $\text{NaLa}(\text{WO}_4)_2$. For the Eu^{3+} emission in the NCs a deviation of mono-exponential decay was observed. A bi-exponential fit reveals a fast initial decay with a decay time of 0.2 ms and a slower component with a 0.64 ms decay. The average lifetime is 0.58 ms. Due to the presence of high energy vibrations (e.g. 3000 cm^{-1} C–H vibration of surface capping molecules) multi-phonon relaxation (MPR) can quench the luminescence. The MPR rate depends on the proximity of C–H vibrations and will vary for Eu^{3+} ions closer to the surface and for those more in the center of the NCs giving rise to a non-exponential decay with a faster initial decay. Possibly, over-

growth with an undoped NaLa(WO₄)₂ layer can reduce the MPR quenching as has been observed for other RE-doped NCs.¹⁷ The long decay component for the Eu³⁺ emission in the NCs of 0.64 ms is longer than the radiative decay time for Eu³⁺ in the MCs (0.54 ms) as a result of the lower effective refractive index resulting in a lower local density of states (LDOS).^{18,19} To vary the emission color and demonstrate the possibility to make a variety of luminescent nanolabels for bio-imaging based on RE-doped NaLa(WO₄)₂ NCs, we also incorporated Tb³⁺ and the Yb³⁺,Er³⁺ upconversion couple in NaLa(WO₄)₂ NCs. In Fig. S7† the emission spectrum of Tb³⁺-doped NCs is shown and for the Er³⁺,Yb³⁺ co-doped sample the upconversion emission spectrum is presented in Fig. S8.†

Conclusions

In conclusion, a one-step thermolysis approach is presented to synthesize complex quaternary NaRE(WO₄)₂ NCs. The small (12 × 29 nm) diamond shaped and ultrathin (~2 nm) NCs are highly monodisperse in apolar solvents. The NCs show oriented attachment along the [001] direction *via* adhesion in the (001) facets of neighboring NCs. The Eu³⁺-doped NCs show the characteristic Eu³⁺ line emission as well as a blue emission that can be assigned to luminescent organic species adsorbed at the NC surface. The presently synthesized luminescent RE-doped NaRE(WO₄)₂ NCs may find applications in transparent luminescent media and bio-imaging while the newly reported synthesis route may serve to aid the development of synthesis routes for other quaternary NCs.

Acknowledgements

This work was financially supported by the “973” Programs (2014CB643801), the Science & Technology Project of Guangdong Province (No. 2015A050502019), the Science & Technology Project of Guangzhou (No. 201510010296), the State Key Laboratory of Optoelectronic Materials and Technologies (Sun Yat-sen University) and the China Scholarship Council (No. 201406385019 and No. 201506380101).

Notes and references

- 1 F. Wang, Y. Han, C. S. Lim, Y. H. Lu, J. Wang, J. Xu, H. Y. Chen, C. Zhang, M. H. Hong and X. G. Liu, *Nature*, 2010, **463**, 1061.
- 2 J. Zhou, Z. Liu and F. Y. Li, *Chem. Soc. Rev.*, 2012, **41**, 1323.
- 3 L. D. Sun, Y. F. Wang and C. H. Yan, *Acc. Chem. Res.*, 2014, **47**, 1001.
- 4 G. F. Wang, Q. Peng and Y. D. Li, *J. Am. Chem. Soc.*, 2009, **131**, 14200.
- 5 J. Wang, R. R. Deng, M. A. MacDonald, B. L. Chen, J. K. Yuan, F. Wang, D. Z. Chi, T. S. A. Hor, P. Zhang, G. K. Liu, Y. Han and X. G. Liu, *Nat. Mater.*, 2014, **13**, 157.
- 6 A. M. Kaczmarek and R. Van Deun, *Chem. Soc. Rev.*, 2013, **42**, 8835.
- 7 Z. J. Wang, J. P. Zhong, H. B. Liang and J. Wang, *Opt. Mater. Express*, 2013, **3**, 418.
- 8 Z. J. Wang, J. P. Zhong, H. X. Jiang, J. Wang and H. B. Liang, *Cryst. Growth Des.*, 2014, **14**, 3767.
- 9 Y. F. Wang, W. Xu, Y. S. Zhu, S. Xu, H. N. Cui and H. W. Song, *J. Mater. Chem. C*, 2014, **2**, 4642.
- 10 X. M. Han, A. García-Cortés, M. D. Serrano, C. Zaldo and C. Cascales, *Chem. Mater.*, 2007, **19**, 3002.
- 11 C. Cascales, A. M. Blas, M. Rico, V. Volkov and C. Zaldo, *Opt. Mater.*, 2005, **27**, 1672.
- 12 C. Cascales, M. D. Serrano, F. Esteban-Betegón, C. Zaldo, R. Peters, K. Petermann, G. Huber, L. Ackermann, D. Rytz, C. Dupré, M. Rico, J. Liu, U. Griebner and V. Petrov, *Phys. Rev. B: Condens. Matter*, 2006, **74**, 174114.
- 13 W. B. Bu, Z. X. Chen, F. Chen and J. L. Shi, *J. Phys. Chem. C*, 2009, **113**, 12176.
- 14 J. D. H. Donnay and D. Harker, *Am. Mineral.*, 1937, **22**, 446.
- 15 Y. S. Fu, X. W. Du, S. A. Kulinich, J. S. Qiu, W. J. Qin, R. Li and J. Sun, *J. Am. Chem. Soc.*, 2007, **129**, 16029.
- 16 C. de Mello Donegá, S. G. Hickey, S. F. Wuister, D. Vanmaekelbergh and A. Meijerink, *J. Phys. Chem. B*, 2003, **107**, 489.
- 17 F. Wang, J. Wang and X. G. Liu, *Angew. Chem., Int. Ed.*, 2010, **49**, 7456.
- 18 T. Senden, F. T. Rabouw and A. Meijerink, *ACS Nano*, 2015, **9**, 1801.
- 19 R. S. Meltzer, S. P. Feofilov, B. M. Tissue and H. B. Yuan, *Phys. Rev. B: Condens. Matter*, 1999, **60**, R14012.